Journal of Fluorescence, Vol. 15, No. 5, September 2005 (© 2005)
DOI: 10.1007/s10895-005-2987-3

Enhanced Fluorescence from Periodic Arrays of Silver Nanoparticles

T. D. Corrigan,[1] S. Guo,[1] R. J. Phaneuf,[1] and H. Szmacinski[2,3]

Received June 4, 2005; accepted July 22, 2005

Electron beam lithography was used to fabricate silver nanoparticle arrays and study the effects of geometrical properties of particles on metal-enhanced fluorescence. Nanoparticle size, shape, interparticle spacing, and nominal thickness were varied in a combinatorial pattern for investigation of the particle plasmon resonance effect on enhancement of fluorescence from three different fluorophores; Fluorescein, Cy3, and Cy5. A specific geometric property for optimal enhancement from each fluorophore was determined. For interparticle spacings greater or equal to 270 nm, the enhancement matched what is expected for a single-particle model. For those particles smaller than 210 nm, the enhancement was lower than for the larger spacing in the range studied. Triangular-shaped particles gave similar enhancement to those of square-shaped particles. This combinatorial pattern by e-beam lithography was found to be useful for studying how individual parameters enhance the fluorescence that are important for rational design of enhanced fluorescence sensors.

KEY WORDS: Fluorescence; particle plasmon resonance; electron-beam lithography; metallic nanoparticles; Cy3; Cy5.

INTRODUCTION

Surface-enhanced spectroscopy originated from observation of surface-enhanced Raman scattering (SERS) in the late 1970s [1,2] prompted scientists to investigate other effects of the enhanced electromagnetic fields near metallic surfaces and colloidal particles. These include enhanced absorption [3,4], luminescence [5,6], and photophysics and photochemistry near metallic surfaces [7,8]. Reviews of these early experimental data and theoretical explanations are given by Moscovits [9] and Wokaun [10]. Most of the experimental investigations to date have centered on SERS since the SERS enhancement was orders of magnitude larger than those observed for fluorescence [11]. Recently, a large interest in exploring of surface-enhanced fluorescence (or metal-enhanced fluorescence) and its applications to biotechnology has been observed [12–19]. In metal-enhanced fluorescence (MEF), the fluorescence signals of molecules placed in the distance of several nanometers from metallic nanostructures can be substantially enhanced. Most of the recently reported experimental work related to MEF was performed using plurality of sizes and shapes of metallic nanoparticles deposited chemically or by vacuum deposition on planar substrates showing that fluorescence over a wide wavelength range can be enhanced. It was demonstrated that such Ag island substrates provide fluorescence enhancement from severalfold to about 100 [12–19]. Such deposited nanoparticle layers are imminently polymorph structures. Broad size and various shape distributions of particles on experimental substrates result in inhomogeneous broadening that blurred the local surface plasmon resonance.

Recent reports on fabrication of ordered arrays of nanoparticles with different sizes, shapes, and interparticle spacing were focused on properties of the particles' plasmon resonance spectra and on SERS but not on

[1] Department of Materials Science and Engineering. University of Maryland and Laboratory for Physical Sciences, College Park, Maryland.
[2] Microcosm Inc., Columbia, Maryland.
[3] To whom correspondence should be addressed. E-mail: henryks@microcosm.com.

1053-0509/05/0900-0777/0 © 2005 Springer Science+Business Media, Inc.

enhanced fluorescence [20–22]. The relation between the geometrical properties of nanoparticle, surrounding environment, and plasmon resonance spectrum were investigated. Also, a theoretical modeling of local fields of particle plasmon resonance for regular [23] and nonregular [24] silver nanoparticles were described and the effects of nanoparticles' shape and size on spectra were reported [20,25] However, to our knowledge there have been no reports systematically studying the effects of varying nanoparticle size and spacing on the fluorescence enhancement of particular fluorophores. This knowledge is important in order to optimize the design of devices that make use of detecting fluorescence from fluorophores, and for practical applications it is necessary to understand which properties give better enhancement for a given wavelength of interest. In order to enhance the design and optimization of MEF, further understanding is needed on the relation between nanoparticle geometrical properties and the enhancement of fluorescence of particular fluorophores. Fluorescein, Cy3, and Cy5 are dyes commonly used in biotechnology applications, especially for microarray technologies. They display different spectral ranges for excitation and emission that allow them to be used in multiplexed studies of wavelength-dependent behavior of metallic nanoparticles and their interactions with excited fluorophores. The optimization process involves finding the condition for which the particle size, shape, and density of the corresponding plasmon wavelength is suitably located at the excitation wavelength or emission wavelength of a selected fluorophore.

To this end we have employed e-beam lithography to investigate the periodic arrays of Ag nanoparticles and their use for fluorescence enhancement. Our approach is the systematic investigation of MEF by independently varying size and interparticle spacing as well as the height of silver nanoparticles by electron beam, lithographically patterning to study the particle plasmon resonance and near field effects on the fluorescence of three spectrally distinctive fluorophores.

EXPERIMENTAL

We use a combinatorial approach in our experiments, creating Ag nanopillars in which the size and spacing are varied from cell to cell. In addition to allowing more simultaneous performance of multiple measurements, this approach allows us to extract the individual dependences of the enhancement while minimizing the variations in fluorophore coverage, thickness of the nanoparticle–fluorophore spacer layer, and incident light intensity which would occur from one experiment to the next. We use Si (001) substrates onto which 25 nm of Al_2O_3 is first deposited to improve adhesion and to avoid fluorescence quenching from proximity to a semiconducting substrate. We spin polymethyl methacrylate onto the substrates, and then expose this layer using a field emission scanning electron microscope (SEM, JEOL JSM-6500F), which has been modified to allow e-beam lithography. The silver was deposited using an e-beam evaporator (CHA Mark 40). We performed fluorescence-enhancement measurements with thicknesses of either 75 or 125 nm, with the upper limit set by the thickness of the PMMA resist. After this, the remaining silver was removed by a lift-off procedure. The geometry of our arrays of silver nanoparticles was varied from cell to cell, with the lateral particle size ranging from 50 to 130 nm and the center-to-center spacing from 150 to 390 nm.

Figure 1a shows an SEM image of part of the array of nanoparticles. A higher magnification view of the 130 nm squares is shown in Fig. 1b. To obtain more accurate height information of the silver nanoparticles, atomic force microscopy was performed. In Fig. 1c, an AFM image and cross-sectional analysis is shown. A plot of the height *vs.* the size is shown in Fig. 1d for the nominally 75 nm deposited film, showing that for the particles with lateral sides of 70 nm and above, the height is pretty uniform (Table I). For smaller nanoparticles (50 nm squares), the film is slightly less in height, but the height variation is only about 4–5 nm.

A finite fluorophore to metal spacing is required to avoid fluorescence quenching [4,26,27]. To define the spacing, we coated the Ag nanoparticle arrays with self-assembled (SAM) spacer layer of BSA-biotin protein approximately 4 nm thick. Fluorescein conjugated to biotin was immobilized using an additional layer of avidin that due to four binding sites for biotin allowed from one side to bind to BSA-biotin and on the other bind fluorescein biotin. The distance of fluorescein to the Ag surface is estimated in this case to be about 9 nm (combined thickness of BSA and Avidin). Cy3 and Cy5 dyes were immobilized to BSA Biotin as streptavidin conjugates. Streptavidin similarly to avidin binds biotin strongly. Both dyes were immobilized simultaneously to the surface using their equimolar mixture. Applying both dyes insured there was no variation in sample preparation and allowed exactly the same areas evaluated using two spectral windows. In Cy3 and Cy5 case the distance from Ag surface is estimated to be about 6.5 nm (BSA and half of streptavidin). Fluorescence images were collected using a laser scanning microscope (LSM 410, Zeiss) with objective magnification of 100× and a numerical aperture of 0.8. For the Fluorescein and Cy3 fluorophores, an Ar ion laser was used for excitation, with both lines at wavelengths of 488

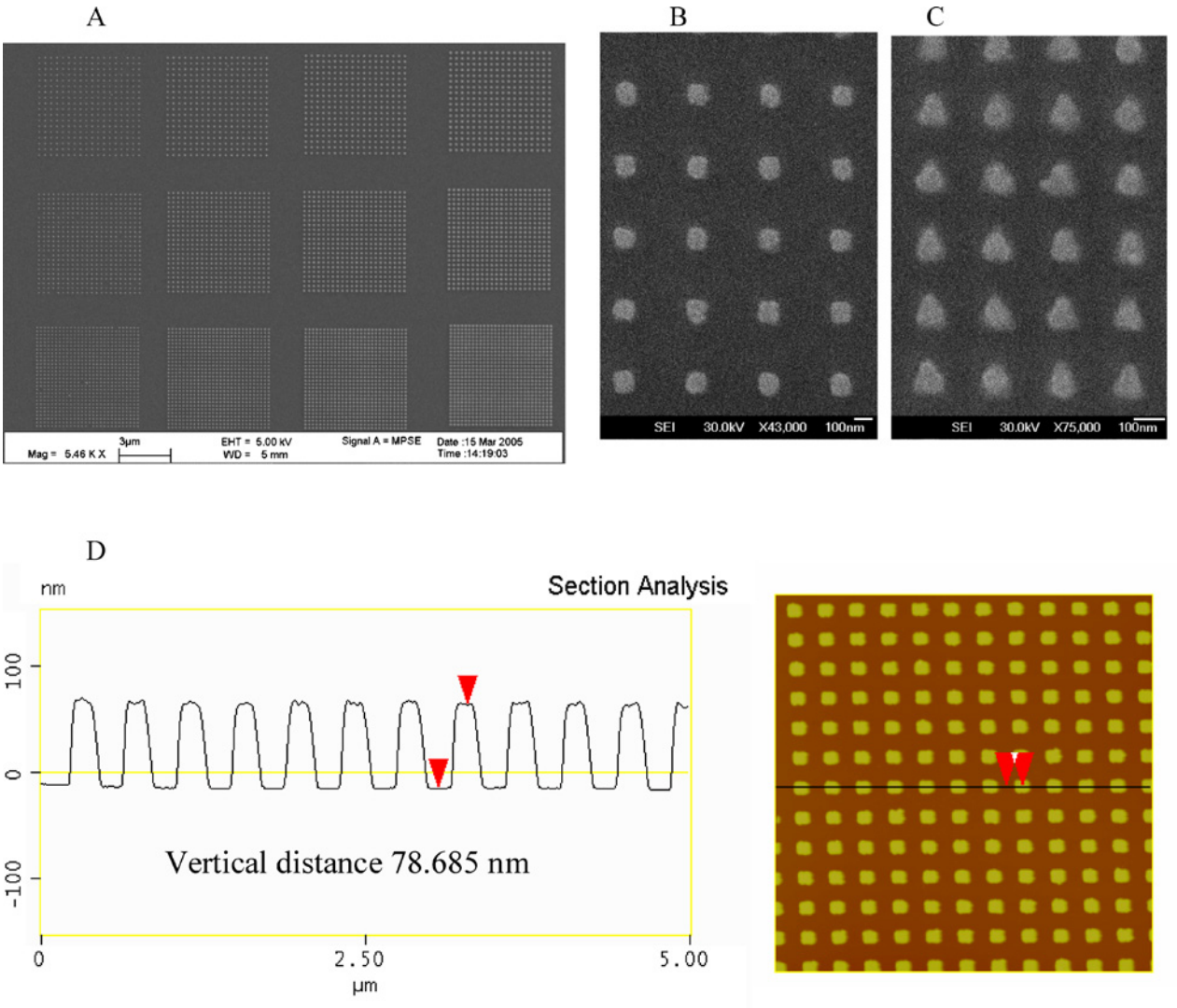

Fig. 1. (A) SEM image of silver nanoparticle arrays. Each squared area represents a combination of the nanoparticle size and interparticle spacing. Each array consisted of 24 or 25 combinations; five sizes and five spacing values (not all shown in the image). (B) A higher magnification SEM image of square nanoparticles with 110 nm lateral size and 390 nm center-to-center interparticle spacing. C) A higher magnification SEM image of triangular nanoparticles with 110 nm lateral size and 210 nm center-to-center interparticle spacing. (D) AFM image and cross-sectional analysis showing the actual height of the particles to be ∼79 nm.

and 514 nm; and the output measured through a filter that passes wavelengths between 535 and 575 nm (Fluorescein) and 575–655 nm (Cy3). For the Cy5 the 633 nm wavelength line of a HeNe laser was used for excitation, while emission was measured through a filter, which passes wavelengths above 660 nm. The absorption and emission spectra of the fluorophores and used excitation wavelengths are shown in Fig. 2. For the first experiment, fluorescein was used alone with an excitation source of 488/514 nm. In the second experiment, intensities of Cy3 and Cy5 were measured alternatively, switching from Cy3 excitation/emission condition to Cy5 using the same sample. Spectroscopic measurements were carried out in a phosphate buffer, pH 7.5.

RESULTS AND DISCUSSION

It is known that the interaction of light with metallic nanoparticles results in extinction spectra where wavelength position and amplitude depend on the size of the particles [22,25]. It is common to provide the extinction or reflectance spectra with characteristics of particle–light interactions. Since the sample areas were very small ($6\,\mu m \times 6\,\mu m$) and Ag particles were deposited on silicon

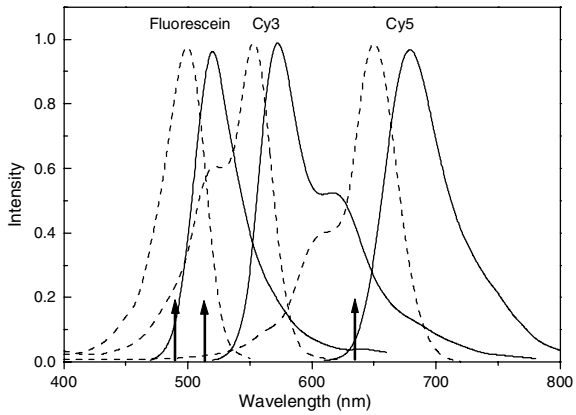

Fig. 2. Absorption and emission spectra of Fluorescein, Cy3, and Cy5. Laser lines used for excitation are shown with arrows: 488 nm, 514 nm, and 633 nm.

wafer (nontransparent), we were not able to measure the extinction spectra directly. Reflectance images at excitation wavelengths were acquired and reflectance relative to the substrate Al_2O_3 were calculated for each patterned array. Figure 3 (top) shows the reflectance images of Ag periodic arrays at two wavelengths for the sample containing 24 combinations of particle sizes and spacings. As expected, the amount of reflected light from the array is dependent on both the size and the periodicity of nanoparticles. It is evident that reflectance images of the same sample are clearly different for two selected wavelengths (see Fig. 3). Darker areas indicate that Ag nanoparticles absorb more light indicating effective particle plasmon resonance. Smaller size of nanoparticles (90–110 nm) absorb more light at 488/514 nm and larger (130 nm) absorb more at 633 nm. It should also be noted that some areas are substantially darker than one would expect from gradual density of nanoparticles. This may include an additional effect of periodicity on reflectance spectra. More detailed reflectance data is shown in Fig. 3 (bottom) where more clearly the minimum reflectance for 488/514 nm corresponds to particle size of 90 nm, and for 633 nm, it corresponds to sizes larger than 130 nm. It was also observed that there was higher reflectance for smaller interparticle spacing and larger particle size (see Fig. 3 and excitation of 633 nm).

Table I. A Silver Nanoparticle Height as Obtained by AFM as a Function of the Lateral Size of the Square Nanoparticles at Deposition Thickness of 75 nm and Spacing of 390 nm

Particle lateral size (nm)	50	70	90	110	130
Particle height (nm)	77.32	80.70	81.66	81.57	82.20

Figure 4 shows the fluorescence images for Cy3 and Cy5. The size/spacing combinatorial method has the advantage that the eye can easily see the arrays of various enhancements. Average intensities were calculated for each array using three samples patterned at identical conditions. Detailed plots of fluorescence enhancement *vs.* the lateral size of the nanoparticles are shown in Figs. 5 and 6. For the similar excitation/emission spectral range, fluorescence enhancement of Cy3 is about twice as large as that of Fluorescein. This difference indicates the interaction of molecules in excited states with Ag nanoparticles that lead to the increased radiative decay rates. Enhancement of Cy3 is expected to be larger than that of Fluorescein because of its smaller quantum efficiency. Another observed effect of the interaction of molecules in excited states is the shift in maximum enhancement toward larger nanoparticle size for Cy3 (B: about 90 nm) compared to Fluorescein (A: about 85 nm). This is because the emission spectrum of Cy3 is at longer wavelengths than Fluorescein. A substantial shift of enhancement maximum toward larger nanoparticles is observed for Cy3 (Fig. 5C), because both excitation and emission are at longer wavelengths. These experimental data are consistent with a red shift in the plasmon resonance with increased lateral size of metallic nanoparticles [22,25].

For triangular Ag nanoparticles the enhancement behavior for Fluorescein and Cy3 (Fig. 6A and B), is similar to that of squared nanoparticles (Fig. 5A and B). A clear shift of maximum enhancement toward larger triangular nanoparticles compared to squared is observed for Cy5, where the size of 130 nm is not yet optimal. Theoretical calculations results in larger plasmon resonance for triangular Ag particles compared to the squared Ag nanoparticles [23], however, in our case we observed similar enhancement factor for both particle shapes. This can be explained that at the distance between fluorophores and the surface of Ag nanoparticles determined by BSA spacer layer, the effective enhanced fields are similar for squared and triangular nanoparticles. While the local field enhancement for triangular-shaped particles is higher at their surfaces, it decays faster with distance than for squared [23]. Thus, the observed effective fluorescence enhancements at distances of 6.5–9 nm are similar for squared and triangular.

Figure 7 shows comparisons of enhancement for selected interparticle spacing of 210 nm for squared and triangular Ag particle arrays with deposition thicknesses of 75 and 125 nm.

A comparison of the peak values shows that the Cy5 fluorescence enhancement is markedly less than the Cy3. Because quantum efficiencies of Cy3 and Cy5 are similar, this may indicate that local field enhancement using

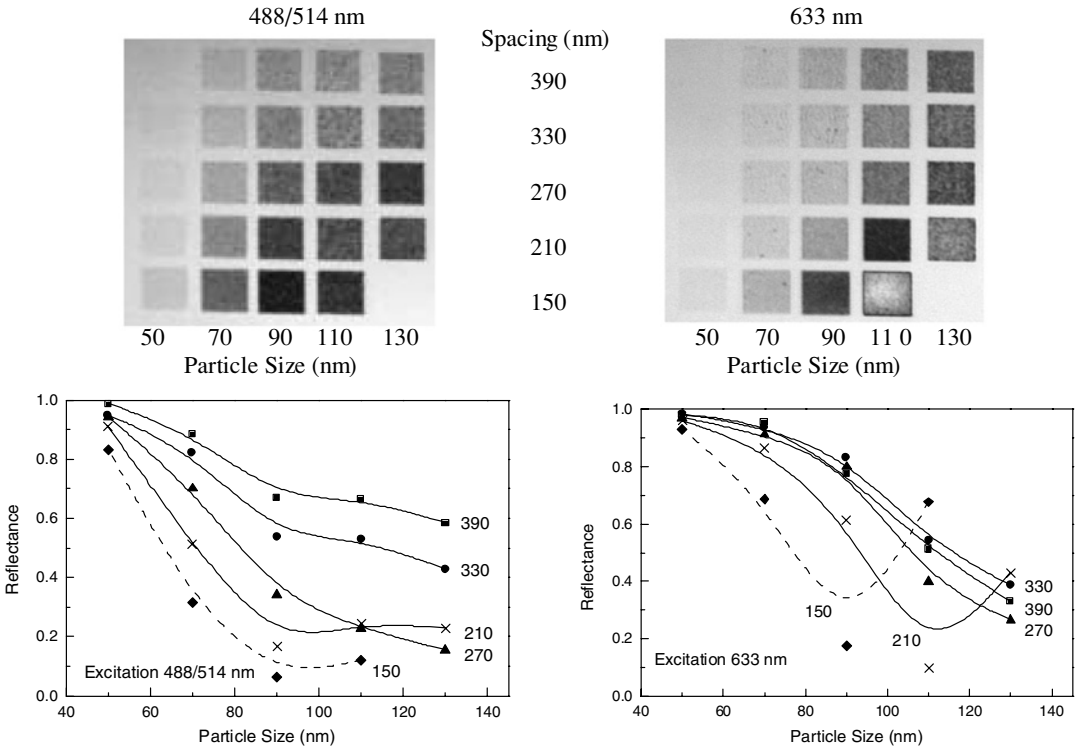

Fig. 3. Top: Reflectance images of Ag periodic arrays with particles height of 125 nm at two excitation wavelengths. Each squared area inside the images consists of unique combination of particle size and interparticle spacing; squared particles with lateral size from 50 to 130 nm (columns from left to right) and center-to-center spacing from 150 to 390 nm (rows from bottom to top). Bottom: Relative reflectance data were calculated for each Ag combination of particle size and spacing.

488/514 nm is larger than using 633 nm. This observation also implies a conclusion that the larger Ag nanoparticles (larger than 110 nm) might be less efficient for fluorescence enhancement as those in the range of 90–100 nm.

From Figs. 5 and 6 it can also be seen that there is a monotonic increase in the metal enhancement as the spacing decreases. This is intuitive when one considers that a smaller spacing means that there is a larger percentage of silver (or more silver nanoparticles) per unit area. Figure 8 presents data normalized to the area of silver. The plot shows that the fluorescence enhancement is very similar for interparticle spacings from 270 to 390 nm. This large interparticle spacing results from the fact that each nanoparticle interacts with excitation light and excited

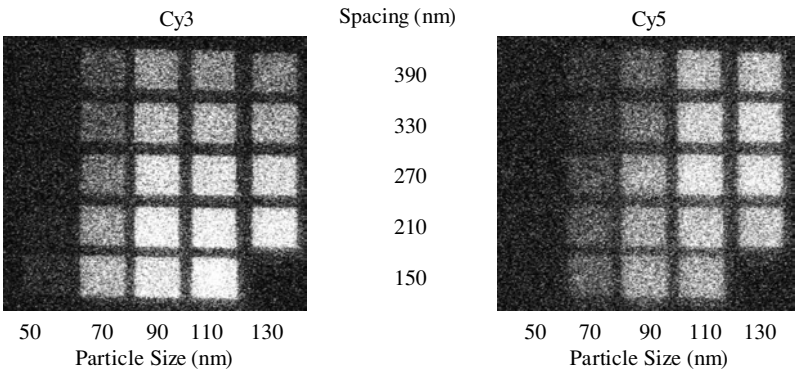

Fig. 4. Intensity images for Cy3 and Cy5 on Ag periodic arrays shown in Fig. 3.

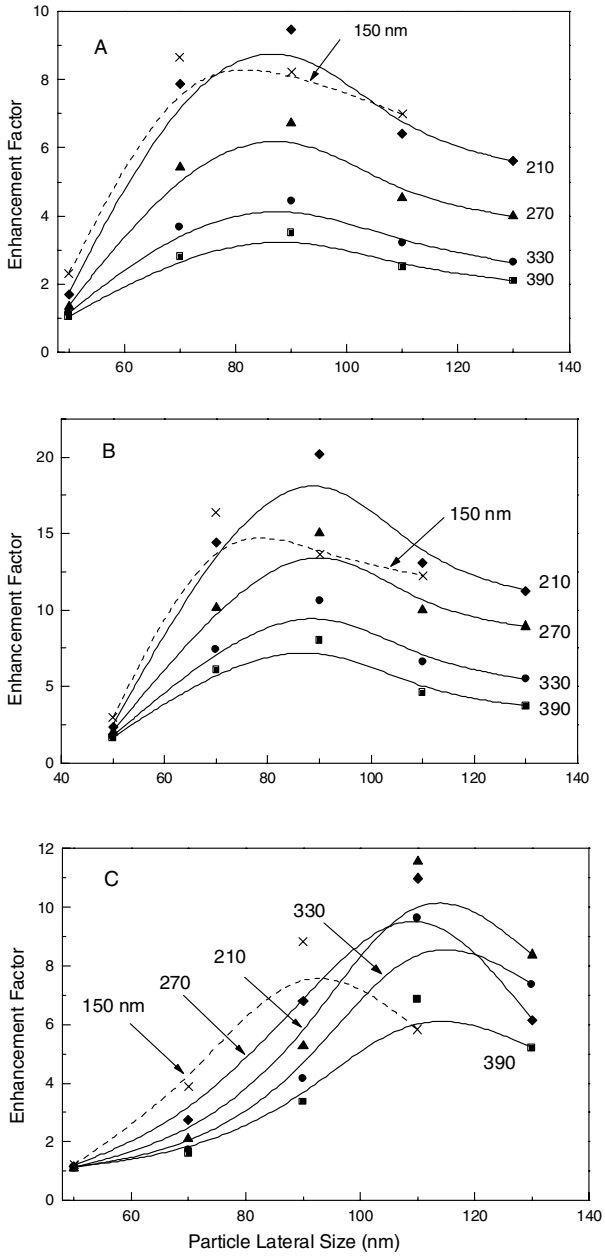

Fig. 5. Fluorescence enhancement for Fluorescein (A), Cy3 (B), and Cy5 (C) using silver nanoparticle arrays of squared shape and deposition thickness of 75 nm.

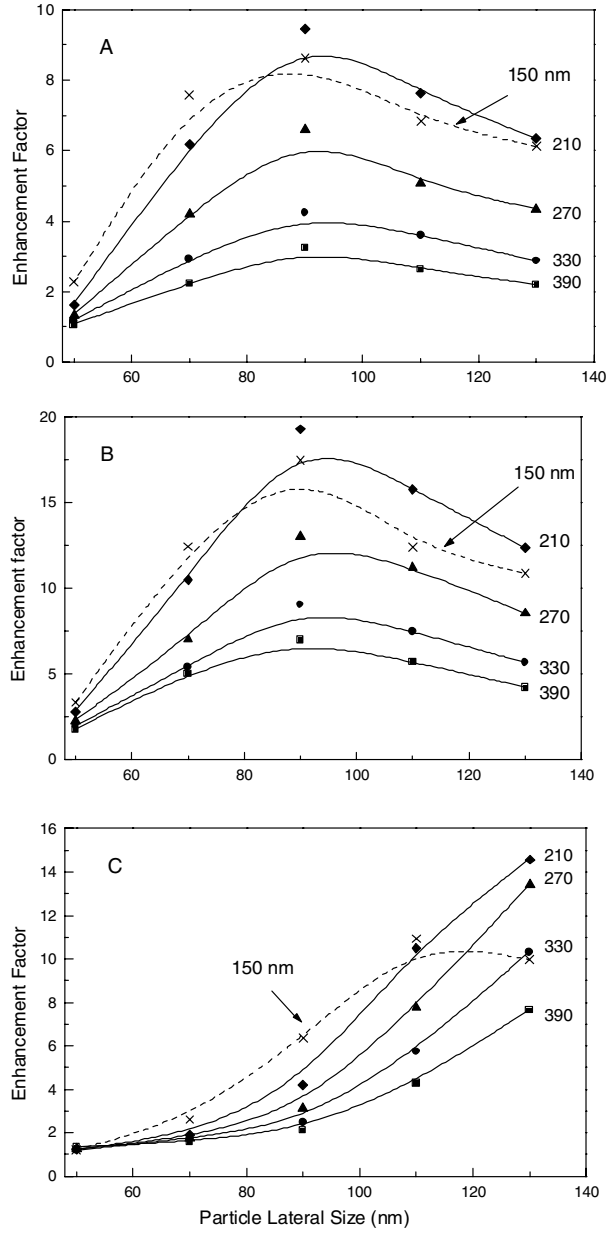

Fig. 6. Fluorescence enhancement for Fluorescein (A), Cy3 (B), and Cy5 (C) using silver nanoparticle arrays of triangular shape and deposition thickness of 75 nm.

molecules as individual particles. We can conclude that at the spacing of about two or more times the lateral size of the nanoparticles, the enhancement no longer has any dependence on spacing (i.e., a single-particle model), thus indicating weak or no coupling between particles. In this case one may predict the optimal conditions for fluorescence enhancement by tuning the size of the nanoparticle (particle plasmon spectrum) to match the spectral properties of the fluorophore. Interestingly, when interparticle spacing is less than 210 nm normalized, the observed enhancements decrease. In this case, due to particle interaction more complex plasmon spectrum is generated than for a single particle. The plasmon spectrum of interacting particles is usually shifted toward longer wavelengths and broadened [21,28]. In order to fully understand the

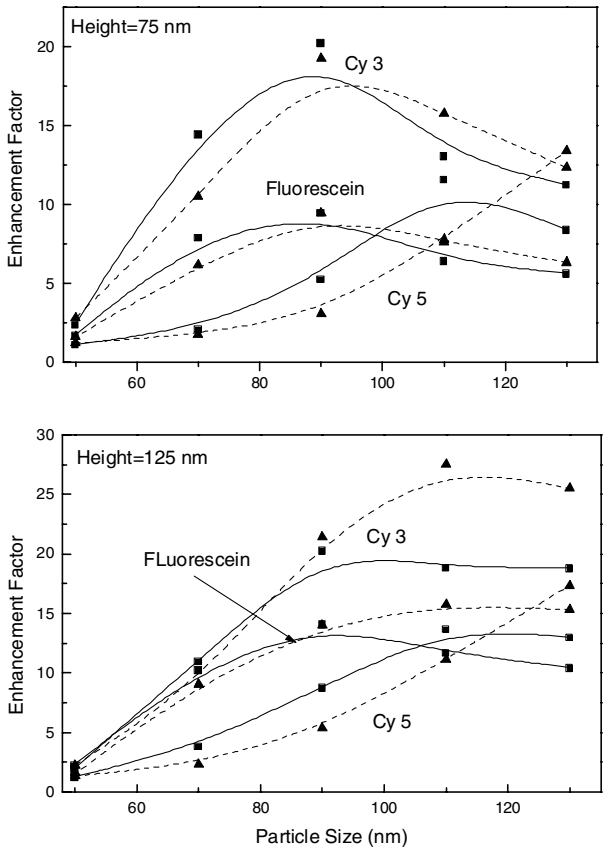

Fig. 7. Comparison of fluorescence enhancements for Fluorescein, Cy 3, and Cy5 observed using Ag nanoparticle arrays of squared and triangular particle shape with two deposition thicknesses of 75 and 125 nm.

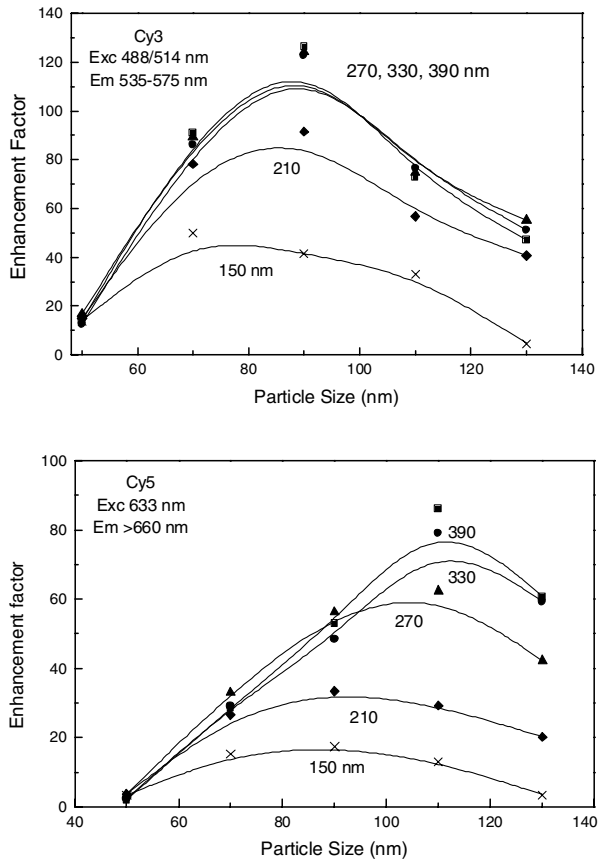

Fig. 8. Fluorescence enhancement normalized to the area of silver within each array. Two spectral ranges are shown, for Cy3 and Cy5. Particle thickness was 125 nm.

rational design of enhanced fluorescence one should also consider recent suggestions of surface plasmon-coupled emission (SPCE) [29] and surface plasmon-coupled directional emission [30].

The strong interaction of excited fluorophores with metallic nanoparticles causes enhanced intensity and decreased fluorescence lifetime as reported by theoretical and experimental data [10,15]. Lifetime data was obtained for Fluorescein–biotin system by acquiring a set of phase-sensitive fluorescence images at modulation frequency of 40 MHz. This was accomplished using Fluorescence Lifetime Imaging Microscope, where sinusoidal modulated amplitude of light emitting diode (LED) and modulated gain of the image intensifier were used [31]. From the difference of the phase angle between fluorescence and excitation signal, a phase lifetime was calculated for each array as $\tau = (1/2\pi f)\, a\tan\theta$, where f is the modulation frequency, and θ the measured phase shift. The average phase lifetime was calculated for each array. Figure 9 shows the fluorescence enhancement and corresponding decrease in lifetime of Fluorescein for arrays of various sizes of triangular and squared Ag with a spacing of 210 nm. The strong relationship between intensity enhancement and decrease in lifetime can be used as direct confirmation of the effects of interaction of excited fluorophore with plasmon-resonant nanoparticles. A large decrease of fluorescence lifetime is observed only for near-field effects, at distances where the excited molecule dipole interacts with the nanoparticle [10,15].

CONCLUSIONS

In conclusion, the method of using electron beam lithography to make a combinatorial pattern was found to be very useful in studying experimentally the effects of Ag nanoparticle geometrical properties on metal-enhanced fluorescence. We have obtained marked average fluorescence enhancement (of the order of 10–20 times) from

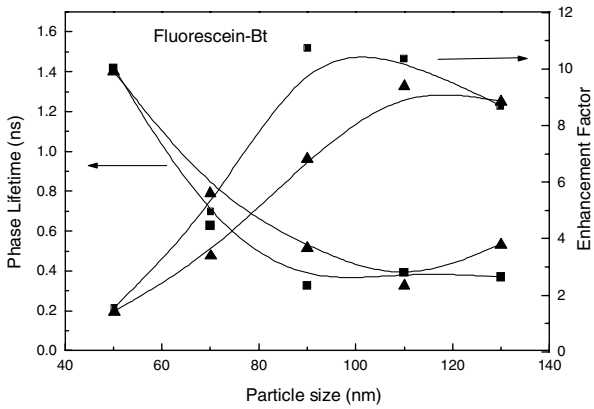

Fig. 9. Decrease in fluorescence lifetime with simultaneous fluorescence enhancemt is a unique fingerprint of interaction of excited molecules with particle plasmon resonance. Data are for Fluorescein–biotin on Ag array with squared and triangular shapes of particles and spacing of 210 nm. Excitations of 470 nm (Blue LED) and modulation frequency of 40 MHz were used.

fluorophores in the presence of ordered arrays of silver nanoparticles and have worked toward understanding the rational design for optimizing the geometric parameters (size, spacing, and thickness) required for particular spectral properties of fluorophores. The optimal enhancement for Fluorescein and Cy3 (excitation 488/514 nm) were obtained for particle size of 85–95 nm. Fluorophores with longer excitation and emission such as Cy5 require larger particles of about 110 nm for greater enhancement. It was found that effective enhancement for squared and triangular-shape Ag nanoparticles are similar with a spacer layer of BSA. For interparticle spacings $\geq$270 nm, the enhancement matched what is expected for a single-particle model. These results can help in the fabrication of devices so that the properties of nanostructures can be tailored depending on the wavelength requirements.

FUTURE WORK

We have studied the effects of the size, shape, spacing, and height of silver nanoparticles on the fluorescence enhancement of three spectrally distinct fluorophores. Another parameter of interest is the effect of polarized light on nonsymmetrical particles as it is predicted that different modes (transversal and longitudinal) may be available for plasmons and therefore may further improve the enhancement. We are currently studying effects of excitation polarization orientation and elongated shapes of particles on the fluorescence enhancement and we are in the process of writing a publication.

ACKNOWLEDGMENTS

This work was supported by the DCI postdoctoral program and the Laboratory for Physical Sciences. We thank Keith Schwab for allowing access to the e-beam lithography system used in fabricating these arrays.

REFERENCES

1. D. L. Jeanmaire and R. P. van Duyne (1977). *J. Electroanal. Chem.* **84**, 1.
2. M. G. Albrecht and J. A. Creighton (1977). *J. Am. Chem. Soc.* **99**, 5215.
3. A. M. Glass, P. F. Liao, J. G. Bergman, and D. H. Olson (1980). *Opt. Lett.* **5**(9), 368–370.
4. S. Garoff, D. A. Weitz, T. J. Gramila, and C. D. Hanson (1981). *Opt. Lett.* **6**(5), 245–247.
5. A. M. Glass, A. Wokaun, J. P. Heritage, J. P. Bergman, P. F. Liao, and D. H. Olson (1981). *Phys. Rev. B* **24**, 4906.
6. G. Ritchie and E. Burstein (1981). *Phys. Rev. B* **24**, 4843.
7. J. I. Gersten and A. Nitzan (1985). *Surf. Sci.* **158**, 165–189.
8. S. Garoff, D. A. Weitz, M. S. Alvarez, and J. I. Nitzan (1984). *J. Chem. Phys.* **81**(11), 5189–5280.
9. M. Moskovitz (1985). *Rev. Mod. Phys.* **57**(3), 783–826.
10. A. Wokaun (1985). *Mol. Phys.* **56**, 1–33.
11. D. A. Weitz, S. Garoff, J. I. Gersten, and A. Nitzan (1983). *J. Chem. Phys.* **78**(9), 5324–5338.
12. K. Sokolov, G. Chumanov, and T. M. Cotton (1998). *Anal. Chem.* **70**, 3998–3905.
13. P. J. Tarcha, J. DeSaja-Gonzales, S. Rodriguez-Llorente, and R. Aroca (1999). *Appl. Spectrosc.* **53**, 43–48.
14. T. Liberman and W. Knoll (2000). *Colloids Surf. A* **171**, 115–130.
15. J. R. Lakowicz (2001). *Anal. Biochem.* **298**, 1–24.
16. N. Stich, A. Gandhum, V. Matushin, C. Maier, G. Bauer, and T. Schalkhammer (2001). *J. Nanosci. Nanotechnol.* **1**(1), 397–405.
17. J. Malicka, I. Gryczynski, and J. R. Lakowicz (2003). *Anal. Chem.* **75**, 4408–4414.
18. J. R. Lakowicz, J. Malicka, I. Gryczynski, Z. Gryczynski, and C. D. Geddes (2003). *J. Phys. D: Appl. Phys.* **36**, R240–R249.
19. F. Yu, D. Yao, and W. Knoll (2003). *Anal. Chem.* **75**, 2610–2617.
20. T. R. Jensen, R. D. Malinsky, C. L. Haynes, and R. P. van Duyne (2000). *J. Phys. Chem. B* **104**, 10549–10556.
21. W. Gotschy, K. Vonmetz, A. Leitner, and F. R. Aussenegg (1996). *Appl. Phys. B* **63**, 381–384.
22. N. Felidj, J. Aubard, G. Levi, J. R. Kren, A. Hohenau, S. Schider, A. Leitner, and F. R. Aussenegg (2003). *Appl. Phys. Lett.* **82**(18), 3095–3097.
23. O. J. F. Martin (2002). In J. Tominaga and D. P. Tsai (Eds.), *Optical Technologies*, Springer, Heidelberg, pp. 203–228.
24. J. P. Kottmann, O. J. F. Martin, D. R. Smith, and S. Schultz (2001). *Phys. Rev. B* **64**, 235402.
25. R. Jin, Y.-W. Cao, C. A. Mirkin, K. L. Kelly, G. C. Schatz, and J. G. Zheng (2001). *Science* **294**, 1901–1903.
26. J. Kummerlen, A. Leitner, H. Brunner, F. R. Ausenegg, and A. Wokaun (1983). *Mol. Phys.* **80**(5), 1031–1046.
27. T. Pal, N. R. Jana, and T. Sau (1997). *Radiat. Phys. Chem.* **49**(1), 127–1130.
28. W. Rechberger, A. Hohenau, A. Leitner, J. R. Kren, B. Lamprecht, and F. R. Aussenegg (2003). *Opt. Commun.* **220**, 137–141.
29. J. R. Lakowicz (2005). *Anal. Biochem.* **337**, 171–194.
30. I. Gryczynski, J. Malicka, Z. Gryczynski, and J. R. Lakowicz (2004). *Anal. Biochem.* **324**, 170–182.
31. H. Szmacinski, J. R. Lakowicz, and M. L. Johnson (1994). *Methods Enzymol.* **240**, 723–748.